UNIVERSITY *of York*

White Rose
university consortium
Universities of Leeds, Sheffield & York

eprints@whiterose.ac.uk
https://eprints.whiterose.ac.uk/

Electron Detachment Dynamics of the Iodide-Guanine Cluster: Does Ionization Occur from the Iodide or from Guanine?

Rosaria Cercola,[1] Kelechi O. Uleanya,[1] and Caroline E. H. Dessent[1]*

1 Department of Chemistry, University of York, Heslington, York, YO10 5DD, UK.

Corresponding author: *ced5@york.ac.uk

RC Orchid: https://orcid.org/0000-0002-2219-6353

KOU Orchid: https://orcid.org/0000-0003-2017-1360

CEHD Orchid: https://orcid.org/0000-0003-4944-0413

Abstract

Laser photodissociation spectroscopy of the I$^-$·guanine complex has been conducted for the first time across the regions above the electron detachment threshold to explore the excited states and whether vertical ionization occurs from the iodide or the nucleobase. The photofragment spectra reveal a prominent dipole-bound excited state (**I**) close to the calculated vertical electron detachment energy (~4.0 eV) and a second excited (**II**) centred around 4.8 eV, which we assign to π-π* nucleobase-localized transitions. The ionic photofragments are identified as I$^-$ and I$^-$·[G-H], with the later fragment being produced significantly more strongly than the former. Both photofragments are observed across the two excited states, with production of the iodide being attributed to internal conversion to the ground state followed by evaporation. We trace the formation of the I$^-$·[G-H] photofragment to initial vertical ionization of guanine, followed by ejection of a proton. This two-step process is important as it follows known steps in radiation-induced damage to DNA, namely initial formation of a guanine radical cation which then forms a free radical [G-H] moiety through deprotonation. Production of the I$^-$·[G-H] photofragment is pronounced through **II** indicating that its formation is enhanced by coupling of the π-π* transitions to the electron detachment continuum.

1. Introduction

Characterising the initial processes that occur in radiation chemistry and biology is an essential part of building a full understanding of the effect of high-energy radiation in condensed matter, including humans and other biological organisms. Ionizing radiation triggers the production of secondary low-energy electrons, chemically reactive species that can attach directly to nucleobases [1]. The resulting nucleobase transient negative ions (TNIs) are important as they can lead to single and double-strand DNA cleavage, as well as the rupture of individual nucleobases. [2,3] Due to the key importance of low-energy electron-nucleobase interactions in these processes, a wide number of experiments and theoretical studies have been performed to probe the key molecular events involved [4-12]. One such series of experiments have involved gas-phase iodide ion-nucleobase clusters. Photoexcitation of these clusters provides a novel route for probing low-energy electron-nucleobase coupling in a highly controlled environment [13-16]. In these experiments, the iodide ion is photodetached to produce a 'spectator' iodine atom and a low-energy free electron with a well-defined kinetic energy that can be captured by an adjacent molecule [17-19]. The resulting TNI dynamics can then be monitored either *via* time-resolved photoelectron spectroscopy or photofragment action spectroscopy [13-21].

The most extensively studied complex to date is that of iodide bound to uracil, i.e. I$^-\cdot$U [15,16,20,21]. Neumark and co-workers performed initial measurements using time-resolved photoelectron spectroscopy, finding that photoexcitation leads to charge transfer from the iodide to the nucleobase, forming a TNI that decays with a biexponential time-profile [20,21]. Subsequent experiments investigated the role played by the spectator iodine [16]. Photodissociation spectroscopy of the cluster produced I$^-$ photofragments as well as deprotonated uracil, i.e. [U-H]$^-$, as a minor photofragmentation channel. Electron production from decay of the TNI was also observed. The production spectra for both photofragment ions displayed two peaks centred at ~4.0 and ~4.8 eV, with the lower-energy band being assigned to a dipole-bound excited state of the complex, while the higher-energy band was primarily assigned to excitation of a π-π* transition localized on the uracil. Crucially, although these excited states are quite distinctive in nature, the time-resolved photoelectron imaging (TRPEI) measurements indicated that across both bands, the I$^-$ ion was being produced *via* internal

3

conversion of the initially formed excited states back to the $I^- \cdot U$ electronic ground state followed by I^- evaporation [20,21].

Further studies have been performed to investigate the electron attachment dynamics in thymine, cytosine and adenine *via* laser photodissociation studies of the $I^- \cdot N$ (N = thymine, adenine, cytosine) clusters [14,15], as well as *via* TRPEI [20,22,23]. These experiments provide a complex picture of the interplay of dipole-bound and valence-anion states formed following near-threshold excitation of the clusters, with the TNIs participating in cluster dissociation following internal conversion back to the electronic ground states. An extensive review of the field has recently been published [13].

In this work, we aim to complete the series of $I^- \cdot N$ nucleobase clusters by presenting the first experimental studies of the $I^- \cdot$guanine cluster, i.e. $I^- \cdot G$. Guanine has been elusive to date since it is extremely difficult to study *via* molecular beam experiments using simple sample heating due to challenges in vaporizing the molecule [11]. Laser desorption provides an alternative route to transferring guanine to the gas phase that has been successfully employed in some experiments [24]. Guanine is also the hardest of the nucleobases to study *via* electrospray ionization due to its low solubility. However, it is a key member of the nucleobase series as it is known to exhibit the lowest ionization energy [25-28], and is renowned for playing a key role in radiation-induced damage of DNA [29,30]. By careful optimization of the electrospray ionization conditions, we have been successful in making $I^- \cdot G$ clusters, therefore allowing us to study this complex *via* laser-induced photodissociation. In the experiments presented here, we aim to establish whether near-threshold ionization results in initial electron loss from the iodide ion or the guanine moiety. Both cases are interesting in the context of the resulting electron dynamics: For iodide photodetachment, the resulting dynamics should involve free electron capture by guanine, whereas in the case where the electron is initially removed from guanine, the experiment may reveal details of a subsequent iodide electron to guanine hole electron transfer.

As a purine base guanine might be expected to exhibit behaviour that is closest to the other purine base, adenine. $I^- \cdot A$ has been investigated by Neumark and co-workers previously *via*

TRPEI of clusters produced in a plasma-ion molecular beam source [23], with two adenine tautomers being observed, the biologically relevant A9 tautomer along with the A3 isomer. In subsequent work from our group where the I$^-$·A clusters were prepared by electrospray ionization, iodide ion clusters with the A7 tautomer were produced [14]. The photodissociation spectra of I$^-$·A displayed a strong dipole-bound excited state, as well as excitations associated with the nucleobase. The overall photofragmentation profiles mirrored those of the pyrimidine clusters, with evidence for nucleobase free electron capture, and internal conversion of the excited states back to hot ground states.

Guanine is known to exist in three common tautomers (9H, 7H or 3H: notation following Ref. [31]), according to the hydrogen atom position (N9, N7 or N3), as well as adopting keto-enol and cis- and trans- conformations. From previous calculations, the 9H- and 7H-keto structures are almost degenerate, with some low-energy enolic forms also existing at relatively low energies [11, 31]. Figure 1 displays the tautomers that are present in our current experiment. Haranczyk and Gutowski have conducted extensive theoretical calculations on the valence and dipole-bound anions of guanine tautomers, finding that the 7H-Enol (7H_E) and 9H-Keto (9H) tautomers can form stable dipole-bound anions. However, they concluded that none of the common guanine tautomers can form adiabatically stable valence anions [11]. Indeed, dissociative electron attachment studies of guanine have revealed that it behaves differently from the other nucleobases, since hydrogen atom loss from the TNI is suppressed compared to single-bond cleavages as well as more complex unimolecular decompositions associated with excision of CN units from the molecular framework [32].

(Figure 1)

2. Methods

UV photodissociation experiments were conducted in a laser-interfaced amaZon SL (Bruker Daltonics) ion-trap mass spectrometer as described previously [33, 34]. The clusters were generated by electrospraying a solution of guanine (1×10^{-4} mol dm^{-3}) mixed with droplets of t-butyl ammonium iodide (1×10^{-2} mol dm^{-3}) solution in deionized water (1×10^{-4} mol dm^{-3}). To increase the solubility of guanine in water, the solution was made alkaline with droplets of a 30% ammonium hydroxide solution. All chemicals were purchased from Sigma Aldrich and used without further purification. Typical operating conditions of our mass spectrometer provide mass resolution better than 0.3 amu.

The I⁻·G clusters were mass-selected and isolated in an ion-trap prior to laser irradiation. UV photons were produced by an Nd:YAG (10 Hz, Surelite) pumped OPO (Horizon) laser across the ranges 326 – 221 nm (3.8 – 5.6 eV). Scans were conducted using a 1 nm step size. The total absorbance of the clusters is presented as photodepletion (PD), which is calculated as the logarithm of the ratio between the ion intensity of mass-selected I⁻·G clusters without and with irradiation. Photodepletion is corrected for the average number of photons used to dissociate the clusters, following Dugourd and co-workers: $\ln(Int_{OFF}/Int_{ON})/(\lambda \cdot P)$ [35]. Here, Int_{ON} and Int_{OFF} are the intensities of the parent clusters with and without irradiation respectively, λ is the irradiation wavelength and P is the average power of the laser. The photodepletion of the clusters was averaged at each scanned wavelength. Photofragment production spectra were recorded at each wavelength and corrected for the cluster intensity as well as the average number of photons i.e. $[Int_{FRAG}/Int_{OFF}]/(\lambda \cdot P)$, where Int_{FRAG} is the intensity of fragment ions produced following photodissociation [35].

Electron detachment (ED) yield spectra were calculated by assuming that any depleted ions not detected as ionic photofragments are decaying by electron detachment, i.e. the electron detachment yield = [(photodepletion ion count – Σ photofragment ion counts)/Int_{OFF}]/($\lambda \cdot P$). This analysis assumes that both the parent ions and photofragments are detected equally in the mass spectrometer, a reasonable assumption for the systems studied here where the parent ions and fragment ions are reasonably close in m/z. In the figure where we present ED spectra (Figure 7), we overlay this data with the photodepletion yield (PD*). PD* is the normalized photodepletion ion count, i.e. PD*= $[(Int_{OFF}-Int_{ON})/Int_{OFF})]/(\lambda \cdot P)$, which provides the most straightforward comparison to the electron detachment yield [14].

The geometric structures of the I⁻·G clusters were studied computationally with Gaussian 09 [36]. Cluster structures of the I⁻ ions coordinated to known guanine isomers were optimised at the B3LYP/6-311++G(2d,2p) level of theory on C, N, O, and H, and 6-311G(d,p) on I, with the iodine core electrons being described using the Stuttgart/Dresden (SDD) electron core pseudopotential. MP2 level calculations were performed to calculate the dipole moments and the spin densities. Cluster binding energies were calculated using the counterpoise correction method. Frequency calculations were performed to ensure that the optimised structures

correspond to true energy minima. To calculate the electronic excitations, time-dependent density functional theory (TD-DFT) calculations (50 states) were performed on the lowest-energy I$^-$·G optimised isomers.

3. Results

3.1 Geometric structures of I$^-$·G

Table 1 lists the relative energies and other calculated properties of the three lowest-energy calculated structures of the I$^-$·G clusters, which are shown in Figure 2. A wide range of additional cluster structures were explored as part of this work, with a selection of the lowest-energy cluster structures being presented in Section S1 of the Supplemental Material (SM). The iodide ion is involved in two hydrogen bonds to the guanine in each of the lowest-energy structures, forming ionic hydrogen-bonds to combinations of the C-H, N-H and O-H groups. (Numerous low-lying cluster isomers have been observed for guanine clusters previously [37].) In the lowest-energy I$^-$·G cluster, guanine is present in the 7H form rather than the 9H canonical form. From a Boltzmann population analysis (Table 1), we expect that all three of the lowest-energy isomers shown in Figure 2 will be present in our electrosprayed ion ensemble. For electrospray from a protic solvent, as used in this study, the isomers should be present at ratios approximately equal to the gas-phase Boltzmann ones [38]. Therefore, we anticipate that I$^-$·G7H will dominate the electrosprayed ion sample (~ 62 %), with I$^-$·G9H also being present at significant levels (~23 %). The I$^-$·G7H_E tautomer is expected to be present as a minor constitutent (~ 15 %).

(Table 1)

For the I$^-$·G clusters studied here, the calculated VDEs are in line with values for the related I$^-$·adenine and I$^-$·pyrimidine [14,15,23]. In the I$^-$·N clusters, detachment results in production of a neutral complex where the iodine atom interacts only very weakly with the nucleobase once the electron is removed. The VDE of the cluster is then effectively blue-shifted from the electron binding energy of the bare iodide ion by the cluster ion-molecule binding energy (~1 eV) [39,40]. We note that our calculated VDEs for the I$^-$·G clusters are also in line with experimental VDEs of Ag$^-$·G and Au$^-$·G clusters measured by Zheng and co-workers [41, 42].

(Figure 2)

7

Figure 3 displays the TD-DFT calculated spectra of the lowest-energy I⁻·G clusters. Such calculations are not expected to accurately predict dipole-bound excited states [15], since tailored, diffuse functionals are necessary to accurately mimic dipole-bound orbitals [43-45]. The TD-DFT calculations predict two bands centred at ~ 4.3 and ~ 5.3 eV for the I⁻·7H cluster (Figure 3a), with a π-π* excitation in each of these bands and a number of charge-transfer (CT) transitions. Similar CT transitions have been calculated previously for other I⁻·nucleobase complexes [14,15]. For the I⁻·G9H cluster (Figure 3b), the calculations predict two strong transitions around 4.8 eV which are associated with two nucleobase-localized π-π* excitation. Between 3.6 to 4.4 eV, a lower-intensity band arises from CT transitions between the *n* orbital on I⁻ and the nucleobase. The spectrum of I⁻·G7H_E (Figure 3c) displays a single strong band over the 3.6-5.0 energy range, which peaks at ~ 4.6 eV and primarily contains a π-π* transition, along with a rising shoulder towards the higher-energy edge since other high-intensity transitions occur at energies above 5.6 eV.

(Figure 3)

3.2 Photodepletion of I⁻·G

Figure 4 shows the photodepletion spectrum of I⁻·G across the range 3.8-5.6 eV. This spectrum corresponds to the gas-phase absorption spectrum of the cluster in the limit where the excited states decay without fluorescence [46]. It is important to note that as the system is anionic, for energies above the detachment energy the photodepletion spectrum (PD) will reflect contributions from electron detachment, as well as intracluster electronic excitations.

(Figure 4)

The I⁻·G photodepletion spectrum displays a somewhat gradual photodepletion onset at ~ 3.8 eV, which is followed by a flat region from 4.1 to 4.5 eV, then another rise in photodepletion around 4.5 eV. Notably, the photodepletion falls above 5.2 eV, back to the level of the 4.1 to 4.5 eV region. The photodepletion onset of 3.8 eV is consistent with the prediction of our calculations, which estimated the VDEs of the two main I⁻·G isomers (I⁻·G7H and I⁻·G9H) as ~ 4 eV. The minor isomer, I⁻·G7H_E, is predicted to have a higher VDE of 4.36 eV, so that the detachment onset for this cluster is likely contributing to the relatively flat appearance of the region between 4.1-4.5 eV. From previous photodepletion spectra of I⁻·nucleobase complexes [14-16], the strong enhancement in photodepletion above 4.5 eV is likely to arise from the presence of guanine-localized transitions. To further explore the nature of the excited states, we next turn to inspecting the action spectra for the photofragments that are produced across the same spectral region.

3.3 Photofragmentation of I$^-$·G

Figure 5 displays the photofragment mass spectra obtained when I$^-$·G is excited at 4.8 and 4.0 eV. At these energies, the two most intense photofragments are the ions with m/z 127 and 277. The m/z 127 photofragment can be straightforwardly assigned to I$^-$, with the m/z 277 ion corresponding to loss of a H atom from the precursor cluster, i.e. either I$^-$·[G-H] or I·[G-H]$^-$. It is likely that the m/z 277 ion is I$^-$·[G-H] rather than I·[G-H]$^-$ as the later cluster is unlikely to be stable given that the neutral I atom would be extremely weakly bound to the deprotonated guanine, and prone to dissociation at thermal energies [47]. We note that [G-H] is a free radical species following H atom loss. At 4.0 eV (Figure 5b), the two photofragments are produced with comparable intensities, but at 4.8 eV (Figure 5a), I$^-$·[G-H] is produced much more strongly than I$^-$ (~10:1). A small number of additional low intensity peaks are evident in the photofragment mass spectra corresponding to the loss of a further one or two H atoms from anionic guanine, or loss of a HNCO unit, a known fragmentation pathway of guanine [32, 48, 49].

(Figure 5)

To gain further insight into the production pathways for the photofragments from I$^-$·G, it is useful to consider their production spectra. Figure 6 displays these spectra, illustrating that the I$^-$ and I$^-$·[G-H] photofragments display somewhat different production spectra, with both displaying fragment production across two regions which we label **I** and **II**. The more intense photofragment I$^-$·[G-H] is produced only weakly across the low-energy spectral region between 3.8-4.2 eV (band **I**), but very strongly across the higher-energy region from 4.4-5.2 eV peaking around 4.8 eV (band **II**). For the less intense I$^-$ photofragment, the fragment action spectrum forms a clear band across the low-energy band **I** region, peaking at 4.0 eV. This energy is notable as it corresponds to the calculated VDEs of the two lowest-energy cluster isomers. I$^-$ is produced with similar intensity through the higher-energy band **II** region with a relatively flat profile, before a fall in intensity towards the high-energy spectral edge.

(Figure 6)

3.4 Electron detachment yield spectra of the X$^-$·A clusters

The electron detachment yield spectrum for I$^-$·G is shown in Figure 7, overlaid with the photodepletion yield (PD*) spectrum for comparison. Both the electron detachment yield and the modified photodepletion spectra largely overlap for I$^-$·G, except between 4.4-5.3 eV (band
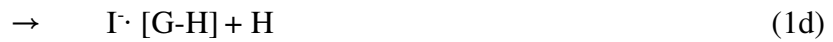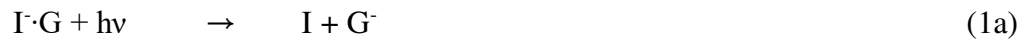
II region). This indicates that ionic photofragmentation is maximised between 4.4-5.3 eV where production of the $I^- \cdot [G-H]$ photofragment is most prominent (Figure 6a). However, even across this region, the difference between electron detachment and photodepletion is small, indicating that electron detachment processes still dominate. This reflects the behaviour of the other $I^- \cdot N$ clusters we have studied [14-16].
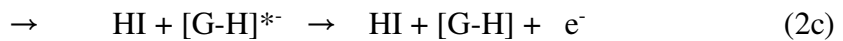
(Figure 7)

4. Discussion

4.1 Overview of the $I^- \cdot G$ Decay Channels

It is useful to review the possible decay pathways for $I^- \cdot G$, prior to discussing the photofragmentation dynamics.   The first group of cluster decay channels result in fragmentation.   For $I^- \cdot G$ this would correspond to pathways such as:

$$I^- \cdot G + h\nu \quad \rightarrow \quad I + G^- \tag{1a}$$

$$\rightarrow \quad I^- + G \tag{1b}$$

$$\rightarrow \quad HI + [G-H]^- \tag{1c}$$

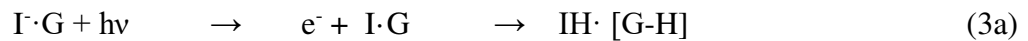$$\rightarrow \quad I^- \cdot [G-H] + H \tag{1d}$$

Alternatively, above the detachment threshold, electron detachment can occur, either *via* direct detachment (2a) or indirectly from an excited state of the cluster (2b). Electron detachment can also occur from hot photofragments, e. g. (2c) and (2d).

$$I^- \cdot G \quad \rightarrow \quad I \cdot G + e^- \tag{2a}$$

$$\rightarrow \quad [I \cdot G]^{*-} \quad \rightarrow \quad [I \cdot G] + e^- \tag{2b}$$

$$\rightarrow \quad HI + [G-H]^{*-} \quad \rightarrow \quad HI + [G-H] + e^- \tag{2c}$$

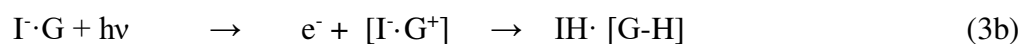$$\rightarrow \quad I + G^{*-} \quad \rightarrow \quad I + G + e^- \tag{2d}$$

An additional possibility occurs when electron detachment leads to the transfer of hydrogen, either as a hydrogen atom or as a proton, on the neutral surface. We observed this process in the $H_2PO_3^- \cdot A$ cluster system [14]. For $I^- \cdot G$, this would result in the following decay pathways:
Hydrogen-atom transfer:

$$I^- \cdot G + h\nu \quad \rightarrow \quad e^- + I \cdot G \quad \rightarrow \quad IH \cdot [G-H] \tag{3a}$$

Proton transfer:

$$I^- \cdot G + h\nu \quad \rightarrow \quad e^- + [I \cdot G^+] \quad \rightarrow \quad IH \cdot [G-H] \tag{3b}$$

10

4.2 Assignment of the I⁻·G excited states

Although no clear bands are evident in the photodepletion spectrum of I⁻·G (Figure 4), the photofragmentation action spectrum of the I⁻·[G-H] photofragment (Figure 6a) clearly shows the presence of two bands (**I** and **II**) which peak at 4.05 and 4.8 eV, respectively. Since 4.05 eV is close to our calculated VDEs for the I⁻·G7H and I⁻·G9H isomers, we assign band **I** to dipole-bound excited states of these two cluster tautomers that are accessed in this region. This assignment is in line with the behaviour of I⁻·N clusters we have studied previously [14-16], and is also consistent with the fact that dipole-bound excited states can be observed *via* photodepletion spectroscopy in our instrument [50,51]. Our calculations indicate that the I⁻·G7H_E isomer should also be present as a minor constituent of our electrosprayed ion ensemble. This cluster isomer is predicted to display a higher VDE (4.36 eV) compared to the keto isomers, in line with its higher dipole moment. We would therefore anticipate that a dipole-bound excited state associated with the I⁻·7H_E isomer should be evident around 4.4 eV, albeit with significantly lower intensity than the I⁻·G7H/ I⁻·G9H dipole-bound excited state. A small enhancement in the photofragmentation action spectra of both the I⁻·[G-H] and I⁻ photofragments (Figure 6) is evident in the region between 4.2-4.35 eV which could be associated with a dipole-bound excited state for the I⁻·G7H_E tautomer.

Band **II**, which is most clearly visible in the I⁻·[G-H] photofragment action spectrum, is centred around 4.8 eV (Figure 6a). This band covers the region of the strong predicted π-π^* transitions for the I⁻·G tautomer clusters (Figure 3), leading us to assign band **II** to nucleobase-centred excitations. This assignment follows those of the other I⁻·N clusters we have studied [14-16]. One further point of note is that there is no prominent spectral signature in either the photodepletion spectrum or photofragmentation spectra of the upper spin-orbit state of the neutral cluster ($^2P_{1/2}$), which should lie 0.94 eV above the $^2P_{3/2}$ state, which is responsible for the band **I** dipole-bound excited state [19,47]. Inspection of the I⁻·G photodepletion spectrum in the region where the $^2P_{1/2}$ state should occur (~5 eV), reveals no evidence of the presence of this new channel opening. It is likely that the appearance of the $^2P_{1/2}$ detachment channel is obscured by strong competitive photoexcitation into the nucleobase localized transitions.
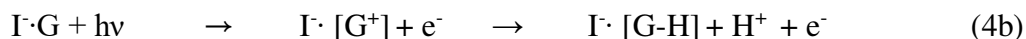
4.3 Photofragment production

Two main mechanisms are normally responsible for the production of ionic photoproducts from anion-nucleobase clusters: The first corresponds to electron transfer from the anion to the nucleobase, whereas the second involves nucleobase-localized electronic excitations [13]. For the case of anion to nucleobase electron transfer, the electron transfer can either be mediated by formation of a dipole-bound excited state or by a direct transfer to a nucleobase valence orbital. When the first type of process occurs, we anticipate that either a guanine anion or deprotonated guanine anion, [G-H]$^-$ will be formed, corresponding to pathways (1a) or (1c), respectively. However, when nucleobase-localised transitions dominate, we expect photoexcitation to be followed by ultrafast decay of the initially populated excited state, and ensuing thermal fragmentation of the electronic ground state. Collision induced dissociation (CID) of the electronic ground state was performed on I$^-$·G to identify the fragments associated with ground-state thermal fragmentation (Section S2 of the SM). CID of I$^-$·G reveals that the cluster fragments with production of I$^-$ as the only ionic fragment, mirroring the behaviour of other iodide-nucleobase complexes [14-16].

The I$^-$·G photofragment action spectra of presented in Section 3.3 revealed that the expected I$^-$ photofragment is produced in the region of the guanine-localised electronic excitations (band **II**). However, it is also produced across the region of the dipole-bound excited state (band **I**). We have observed this phenomenon previously, as all of the iodide-pyrimidine clusters produce I$^-$ as a photofragment through the regions of their near-threshold dipole-bound excited state. This behaviour has been attributed to internal conversion to the ground electronic state followed by evaporation of I$^-$ [15, 16].

While photofragmentation of I$^-$·G into I$^-$ mirrors other iodide-nucleobase clusters, I$^-$·[G-H] type photofragments have not been observed previously. Indeed, formation of this fragment cannot be attributed to a mechanism involving electron transfer from iodide to guanine, as such a process would have resulted in dissociative attachment fragments associated with free energy electron attachment to guanine. This leads us to consider alternative photofragmentation mechanisms for production of I$^-$·[G-H]. In discussing this photofragment, it is important to acknowledge that it could be formed by two routes, either direct ejection of a hydrogen atom (4a) or ionization of an electron from guanine to form a CT state, followed by ejection of a proton (4b):

$$I^- \cdot G + h\nu \quad \rightarrow \quad I^- \cdot [G-H] + H \tag{4a}$$

Or,

$$I^- \cdot G + h\nu \quad \rightarrow \quad I^- \cdot [G^+] + e^- \quad \rightarrow \quad I^- \cdot [G\text{-}H] + H^+ + e^- \quad (4b)$$

We note that (4b) represents a two-step version of the pathway depicted in pathway (1d) in Section 4.1.

It seems unlikely that pathway (4a) is followed given that it is not active in the other $I^- \cdot N$ clusters. This suggests that pathway (4b) is leading to $I^- \cdot [G\text{-}H]$ formation. Guanine is well known as being distinguished from the other nucleobases by having a considerably lower ionization energy. This was first demonstrated unequivocally by Wang and co-workers in their photodetachment studies of gaseous nucleotide anions, where the guanine nucleotides were observed to display much lower ionization energies than the other nucleotides [27]. These experiments were supported by Chatterly and co-workers in two-photon ionization measurements on nucleotides [52], where the guanine-containing nucleotide was the only system where ionization occurred from the base. Indeed, it is well acknowledged that guanine sites within DNA and nucleotides have the greatest propensity to be ionized [25-28], and a number of studies have revealed that ionizing radiation causes positive hole formation at guanine sites [53-57]. The photophysics and dynamics of these DNA charge-separated states are of key current interest [58,59].

To further explore whether the guanine within $I^- \cdot G$ is the site of vertical ionization, spin density calculations if $I^- \cdot G$ were conducted for the key tautomers, with the results presented in Figure 8. The calculations reveal that the electron is indeed removed from guanine upon vertical ionization for all three tautomers, in striking contrast to the previously studied $I^- \cdot A$ cluster, where spin-density calculations were also conducted and revealed that the ionized electron was removed from the iodide [14].

(Figure 8)

In our experiment, we are not able to directly detect $I^- \cdot [G^+]$ since this CT complex is neutral. To form the detected $I^- \cdot [G\text{-}H]$ cluster, the CT complex must subsequently eject a proton, as shown in the second step of pathway (4b). This is not unreasonable given that the CT complex is likely to contain substantial excess energy, as well as the fact that guanine radical cations are known to undergo rapid decay via proton loss [60-62].

13

5. Further discussion

The I⁻·G cluster is distinctive compared to the other I⁻·nucleobase clusters as it produces I⁻·[G-H] as a relatively strong photoproduct. The origin of this photofragment appears to lie in the low ionization potential of guanine compared to the other nucleobases. This leads to the initial ionization site within I⁻·G being localized on the guanine molecule, producing a charge-separated product which subsequently decays *via* loss of a proton from the guanine radical cation within the cluster. This explanation fits well with the known ionization behaviour of guanine in gaseous nucleotides [27,52]. However, what is surprising in this context is the fact that the photophysics of the I⁻·G cluster are remarkably similar to those of the other I⁻·nucleobase clusters. This is true in relation to the fact that the photofragment action spectra indicate the presence of two excited states for the cluster with a near-threshold dipole-bound excited state and a higher-energy excited state that can be linked to nucleobase localized transitions. The fact that a dipole-bound state exists for the I⁻·G cluster despite the guanine moiety being the electron source, can be attributed to little geometric rearrangement in the cluster upon vertical ionization. It is also notable that production of the distinctive I⁻·[G-H] photofragment is strongly enhanced in the region where excitation of the guanine π-π* transitions are dominant. It seems that electron detachment (and hence production of I⁻·[G-H]) is being enhanced by coupling of the π-π* transitions to the electron detachment continuum. This effect mirrors the coupling of the analogous π-π* transitions to the electron detachment continuum in other I⁻·nucleobase clusters [14-16], and in $Pt(CN)_{4,6}^{2-}$·nucleobase complexes [63, 64].

I⁻·G represents an important test case for future time-resolved studies to confirm whether guanine is indeed the vertical ionization site, and explore the CT state dynamics. Time-resolved studies are particularly relevant for this cluster given that guanine bases are known to be the primary sites of radiation damage in DNA through initial formation of radical cations [54-59]. The primary photofragmentation channel identified for I⁻·G in this study mimics this key process, and thus demonstrates that the cluster is a key model system for further experimental and theoretical studies.

References

[1] S. Lehnert, Biomolecular Action of Ionizing Radiation, 1st ed. (CRC Press, Boca Raton, FL, 2007).

[2] E. Alizadeh and L. Sanche, Chem. Rev. **112**, 5578 (2012).

[3] L. Sanche, Eur. Phys. J. D **35**, 367 (2005).

[4] Y. Dong, Y. Gao, W. Liu, T. Gao, Y. Zheng, and L. Sanche, J. Phys. Chem. Lett. **10**, 2985 (2019).

[5] S. Denifl, S. Ptasinska, G. Hanel, B. Gstir, M. Probst, P. Scheier, and T. D. Mark, J. Chem. Phys. 120, **14**, (2004).

[6] J. Ameixa, E. Arthur-Baidoo, R. Meißner, S. Makurat, W. Kozak, K. Butowska, F. Ferreira da Silva, J. Rak, and S. Denifl, J. Chem. Phys. **149**, 164307 (2018).

[7] J.K. Wolken and F. Turecek, J. Am. Chem. Soc. **123**, 5804 (2001).

[8] J.H. Hendricks, S.A. Lyapustina, H.L. de Clercq, J.T. Snodgrass, and K.H. Bowen, J. Chem. Phys. **104**, 7788 (1996).

[9] J. Simons, Acc. Chem. Res. **39**, 772 (2006).

[10] H.Y. Chen, P.Y. Yang, H.F. Chen, C.L. Kao, and L.W. Liao, J. Phys. Chem. B **118**, 11137 (2014).

[11] M. Haranczyk and M. Gutowski, J. Am. Chem. Soc. **127**, 699 (2005).

[12] M.A. Fennimore and S. Matsika, J. Phys. Chem. A **122**, 4048 (2018).

[13] A. Kunin and D.M. Neumark, Phys. Chem. Chem. Phys. **21**, 7239 (2019).

[14] R. Cercola, E. Matthews and C.E.H. Dessent, Mol. Phys. **117**, 3001 (2019).

[15] E. Matthews, R. Cercola, G. Mensa-Bonsu, D.M. Neumark and C.E.H. Dessent, J. Chem. Phys. **148**, 084304 (2018).

[16] W.L. Li, A. Kunin, E. Matthews, N. Yoshikawa, C.E.H. Dessent and D.M. Neumark, J. Chem. Phys. **145**, 044319 (2016).

[17] C.E H. Dessent, C.G. Bailey and M.A. Johnson, J. Chem. Phys. **105**, 10416 (1996).

[18] C.E.H. Dessent, J. Kim and M.A. Johnson, Faraday Discuss. **115**, 395 (2000).

[19] F. Mbaiwa, M. Van Duzor, J. Wei and R. Mabbs, J. Phys. Chem. A **114**, 1539 (2009).

[20] S.B. King, M.A. Yandell, and D.M. Neumark, Faraday Disscuss. **163**, 59 (2013).

[21] S.B. King, M.A. Yandell, A.B. Stephansen and D.M. Neumark, J. Chem. Phys. **141**, 224310 (2014).

[22] S.B. King, A.B. Stephansen, Y. Yokoi, M.A. Yandell, A. Kunin, T. Takayanagi and D.M. Neumark, J. Chem. Phys. **143**, 024312 (2015).

[23] A.B. Stephansen, S.B. King, Y. Yokoi, Y. Minoshima, W.L. Li, A. Kunin, T. Takayanagi and D.M. Neumark, J. Chem. Phys. **143**, 104308 (2015).

[24] S. Boldissar and M.S. de Vries, Phys. Chem. Chem. Phys. **20**, 9701 (2018).

[25] V. Palivec, E. Pluhařová, I. Unger, B. Winter and P. Jungwirth, J. Phys. Chem. B **118**, 13833 (2014).

[26] D. Roca-Sanjuán, M. Rubio, M. Merchán, and L. Serrano-Andrés, J. Chem. Phys. **125**, 084302 (2006).

[27] X. Yang, X.B. Wang, E.R. Vorpagel and L.S. Wang, Proc. Natl. Acad. Sci. U. S. A. **101**, 17588 (2004).

[28] E. Palecek and M. Bartosik, Chem. Rev. **112**, 3427 (2012).

[29] S. Kanvah, J. Joseph, G.B. Schuster, R.N. Barnett, C.L. Cleveland and U. Landman, Acc. Chem. Res. **43**, 280 (2010).

[30] F.D. Lewis, R.L. Letsinger, and M.R. Wasielewski, Acc. Chem. Res. **34**, 159 (2001).

[31] G. Chung, H.B. Oh and D. Lee, J. Mol. Struct. THEOCHEM **730**, 241 (2005).

[32] H. Abdoul-Carime, J. Langer, M.A. Huels, and E. Illenberger, Eur. Phys. J. D **35**, 399 (2005).

[33] E. Matthews, A. Sen, N. Yoshikawa, E. Bergstrom and C.E.H. Dessent, Phys. Chem. Chem. Phys. **18**, 15143 (2016).

[34] A. Sen, T.F.M. Luxford, N. Yoshikawa and C.E.H. Dessent, Phys. Chem. Chem. Phys. **16**, 15490 (2014).

[35] I. Compagnon, A.R. Allouche, F. Bertorelle, R. Antoine and P. Dugourd, Phys. Chem. Chem. Phys. **12**, 3399 (2010).

[36] M.J. Frisch, G.W. Trucks, H.B. Schlegel, G.E. Scuseria, M.A. Robb, J.R. Cheeseman, G. Scalmani, V. Barone, B. Mennucci, G.A. Petersson, H. Nakatsuji, M. Caricato, X. Li, H.P. Hratchian, A.F. Izmaylov, J. Bloino, G. Zheng, J.L. Sonnenberg, M. Hada, M. Ehara, K. Toyota, R. Fukuda, J. Hasegawa, M. Ishida, T. Nakajima, Y. Honda, O. Kitao, H. Nakai, T. Vreven, J.J.A. Montgomery, J.E. Peralta, F. Ogliaro, M. Bearpark, J.J. Heyd, E. Brothers, K.N. Kudin, V.N. Staroverov, R. Kobayashi, J. Normand, K. Raghavachari, A. Rendell, J.C. Burant, S.S. Iyengar, J. Tomasi, M. Cossi, N. Rega, J.M. Millam, M. Klene, J.E. Knox, J.B. Cross, V. Bakken, C. Adamo, J. Jaramillo, R. Gomperts, R.E. Stratmann, O. Yazyev, A.J. Austin, R.

Cammi, C. Pomelli, J.W. Ochterski, R.L. Martin, K. Morokuma, V.G. Zakrzewski, G.A. Voth, P. Salvador, J.J. Dannenberg, S. Dapprich, A.D. Daniels, O. Farkas, J.B. Foresman, J.V. Ortiz, J. Cioslowski and D.J. Fox, Gaussian 09, Revision D.01 (Gaussian, Wallingford, CT, 2009).

[37] M. Schreiber and L. Gonzalez, J. Comput. Chem. **28**, 2299 (2007).

[38] E. Matthews and C. E. H. Dessent, Phys. Chem. Chem. Phys. **19**, 17434 (2017).

[39] C.E.H. Dessent, C. G. Bailey and M. A. Johnson, J. Chem. Phys. **103**, 2006 (1995).

[40] A.W. Castleman Jr and K.H. Bowen Jr, J. Phys. Chem. **100**, 12911 (1996).

[41] G.J. Cao, H.G. Xu, X.L. Xu, P. Wang and W.J. Zheng, Int. J. Mass Spectrom. **407**, 118 (2016).

[42] G.J. Cao, H.G. Xu, W.J. Zheng and J. Li, Phys. Chem. Chem. Phys. **16**, 2928 (2014).

[43] W.J. Morgan and R.C. Fortenberry, Theor. Chem. Acc. **134**, 47 (2015).

[44] P. Skurski, M. Gutowski and J. Simons, Int. J. Quantum Chem. **80**, 1024 (2000).

[45] J. Simons, Annu. Rev. Phys. Chem. **62**, 107 (2011).

[46] S.M.J. Wellman and R.A. Jockusch, J. Phys. Chem. A. **119**, 6333 (2015).

[47] C.C. Arnold, D.M. Neumark, D.M. Cyr and M.A. Johnson, J. Phys. Chem. **99**, 1633 (1995).

[48] L. Sadr-Arani, P. Mignon, H. Chermette, H. Abdoul-Carime, B. Farizon, M. Farizon, Phys. Chem. Chem. Phys. **17**, 11813 (2015).

[49] A. Ostroverkh, A. Zavilopulo and O. Shpenik, Eur. Phys. J. D **73**, 38, (2019).

[50] A.J.A. Harvey, N. Yoshikawa, J.G. Wang and C.E.H. Dessent, J. Chem. Phys. **143**, 101103 (2015).

[51] E. Matthews and C.E.H. Dessent, J. Phys. Chem. Lett. **9**, 6124 (2018).

[52] A.S. Chatterley, A.S. Johns, V.G. Stavros, and J.R.R. Verlet, J. Phys. Chem. A **117**, 5299 (2013).

[53] R. Chakraborty and D. Ghosh, Phys. Chem. Chem. Phys. **18**, 6526 (2016).

[54] Y. Rokhlenko, N. E. Geacintov, V. Shafirovich, J. Am. Chem. Soc. **134**, 4955 (2012).

[55] T. Melvin, S.M.T. Cunniffe, P. O'Neill, A.W. Parker and T. Roldan-Arjona, Nucleic Acids Res. **26**, 4935 (1998).

[56] A. Adhikary, D. Khanduri and M. D. Sevilla, J. Am. Chem. Soc. **131**, 8614 (2009).

[57] M.K. Kuimova, A.J. Cowan, P. Matousek, A.W. Parker, X.Z. Sun, M. Towrie, and M.W. George, Proc. Natl. Acad. Sci. U.S.A **103**, 2150 (2006).

[58] J. Jie, K. Liu, L. Wu, H. Zhao, D. Song, and H. Su, Sci. Adv. **3**:e170017 (2017).

[59] E. Balanikas, A. Banyasz, G. Baldacchino and D. Markovitsi, Molecules **24**, 2347 (2019).

[60] M. D. Sevilla, A. Kumar, and A. Adhikary, J. Phys. Chem. B **120**, 2984 (2016).

[61] O.B. Morozova, N.N. Fishman and A.V. Yurkovskaya, Phys. Chem. Chem. Phys. **19**, 21262 (2017).

[62] K. Kobayashi and S. Tagawa, J. Am. Chem. Soc. **125**, 10213 (2003).

[63] A. Sen and C. E. H. Dessent, J. Phys. Chem. Lett. **5**, 3281 (2014).

[64] A. Sen, E. Matthews, G. Hou, X. Wang and C. E. H. Dessent, J. Chem. Phys. **143**, 184307 (2015).

Table 1. Properties of the $I^- \cdot G$ clusters calculated at the B3LYP/6-311++G(2d,2p) level of theory, with 6-311G(d,p)/SDD for I^-.

Cluster	Relative Energy kJ mol⁻¹	Boltzmann population[a] %	VDE Calc. eV	Vertical Dipole Moments[b]	Binding Energy kJ mol⁻¹
$I^- \cdot G7H$	0.0	61.6	4.05	8.7	-95.5
$I^- \cdot G9H$	2.4	23.1	4.02	19.8	-94.9
$I^- \cdot G7H\_E$	3.5	15.3	4.36	11.6	-121.2

[a] At 298 K.

[b] At the MP2/6-311++G(2d,2p) level of theory, with 6-311G(d,p)/SDD for I^-.
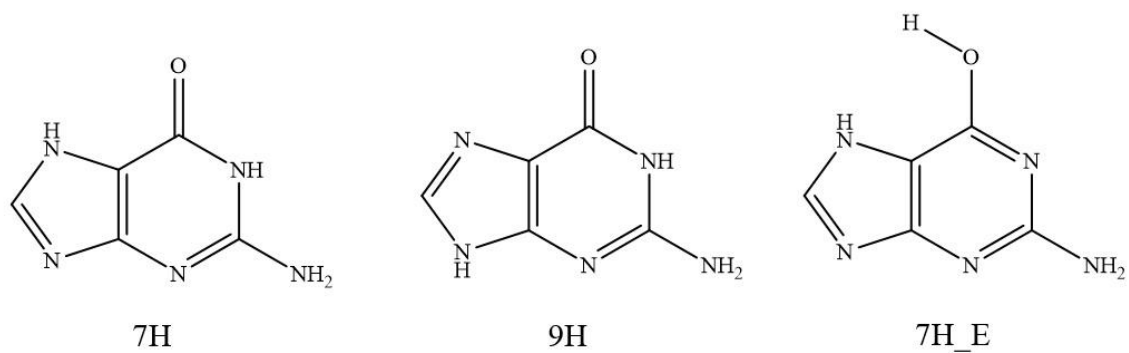
Figure 1
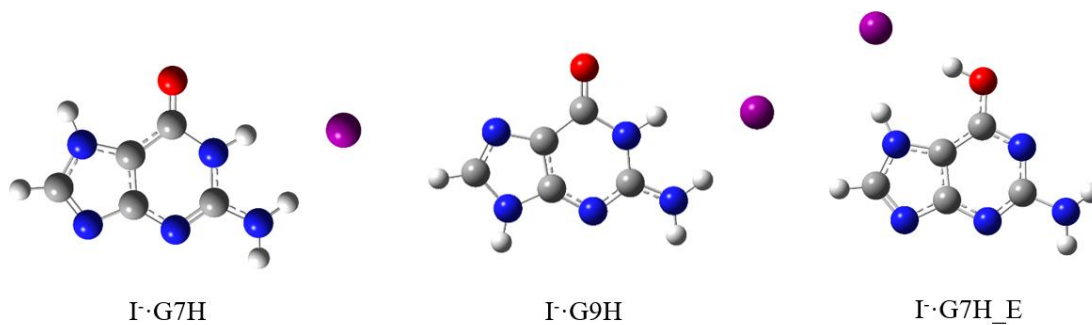
Figure 2
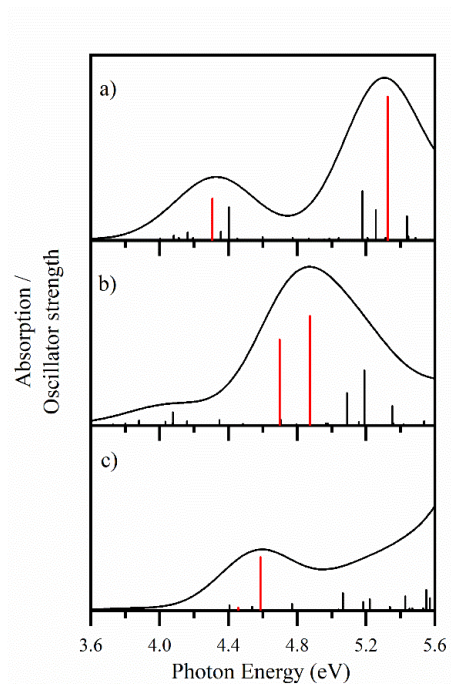
Figure 3
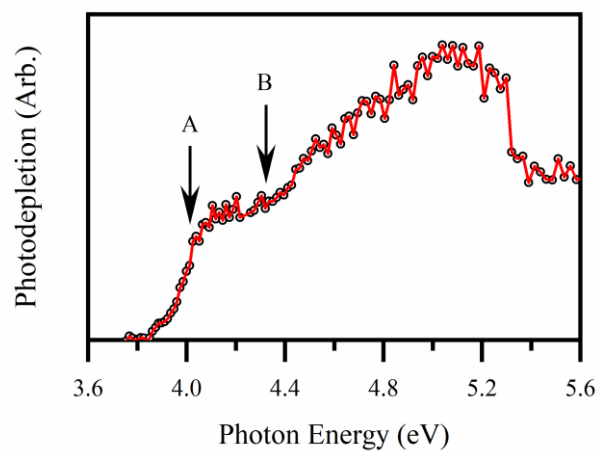
Figure 4
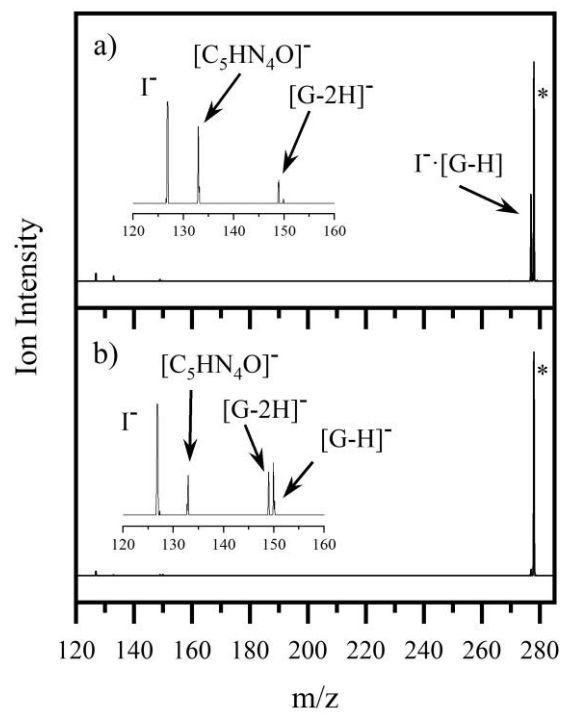
Figure 5

Figure 6

Figure 7

I⁻·G7H   I⁻·G9H   I⁻·G7H_E
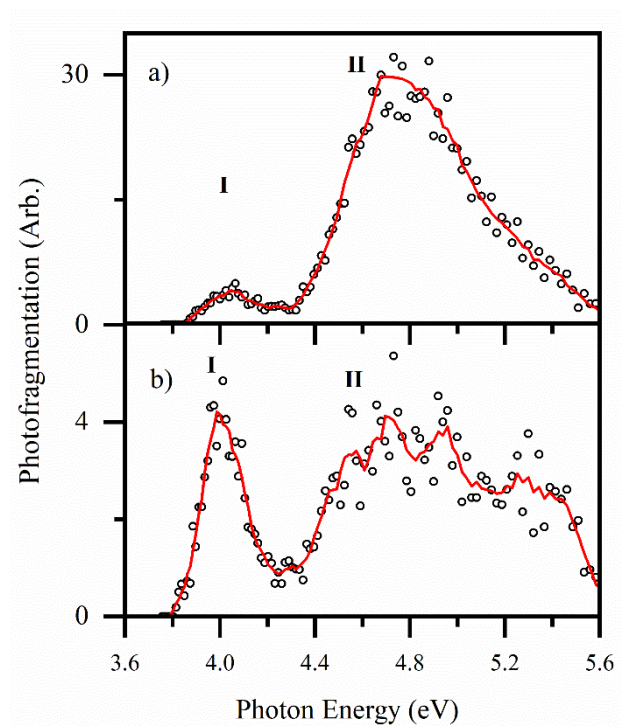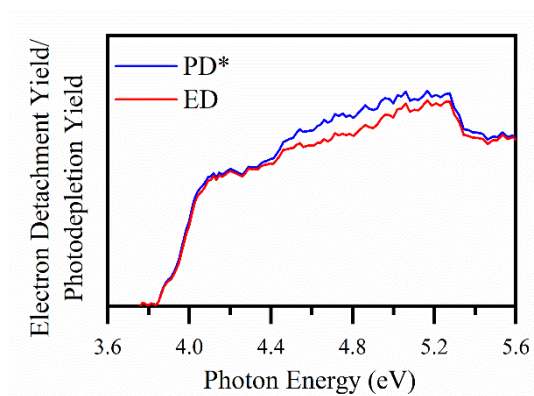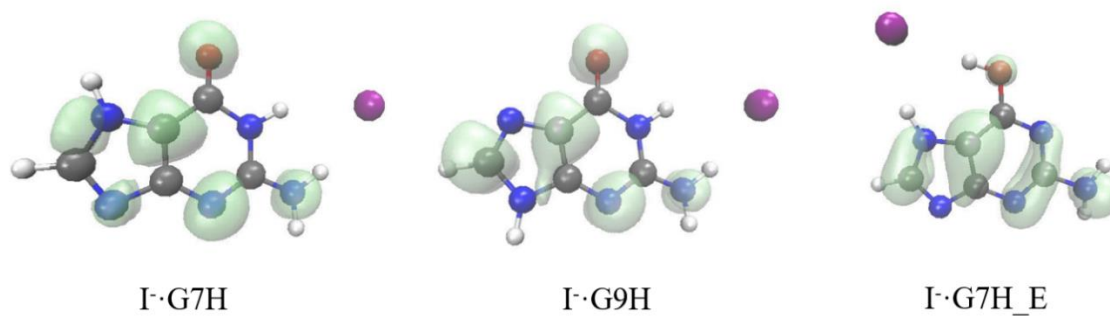
Figure 8

Figure 1. Structures of the 7H-keto (7H), 9H-keto (9H) and 7H-enol (7H_E) tautomers of guanine.

Figure 2. The lowest-energy structures of the I·G clusters, calculated at the B3LYP/6-311++G(2d,2p) level of theory, with 6-311G(d,p)/SDD for I⁻.

Figure 3. TD-DFT calculated spectra (50 states) of (a) I·G7H (b) I·G9H and (c) I·G7H_E. The oscillator strengths of the strongest transitions are given by the vertical bars. Red lines denote π-π* transitions, whereas black lines denote charge transfer transitions from the iodide. The full black line spectrum represents a convolution of the calculated transitions with a Gaussian function (0.25 eV HWHM).

Figure 4. Photodepletion spectrum of the I·G cluster. The line is a five-point adjacent average of the data points. Arrow A indicates the calculated VDEs of the I·G7H and I·G9H isomers, with arrow B indicating the calculated VDE of I·G7H_E.

Figure 5. Photofragment mass spectra of the I·G cluster obtained at (a) 4.8 and (b) 4.0 eV. The peak labelled * is the I·G precursor ion.

Figure 6. (a) I·[G-H] and (b) I⁻ photofragment action spectra produced from the I·G cluster. The line is a five-point adjacent average of the data points.

Figure 7. Photodepletion yield (PD*) and electron detachment yield (ED) of the I·G cluster. The curves displayed are three points adjacent average of the data points. PD* and ED are defined in Section 2.

Figure 8. Spin-density plots of the I·G7H, I·G9H and I·G7H_E tautomers of I·G. The shaded regions indicate areas where excess electro-spin density is located following ionization.

Supplemental Material

Electron Detachment Dynamics of the Iodide-Guanine Cluster: Does Ionization Occur from the Iodide or from Guanine?

Rosaria Cercola,[1] Kelechi O. Uleanya,[1] and Caroline E. H. Dessent[1]*

[1] Department of Chemistry, University of York, Heslington, York, YO10 5DD, UK.

S1 Lowest Energy $I^-\cdot G$ clusters
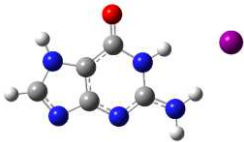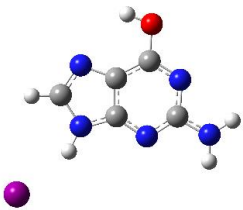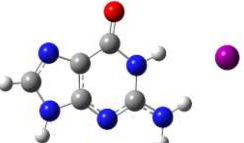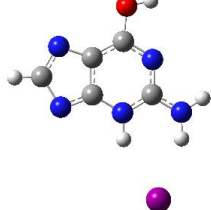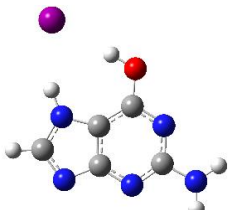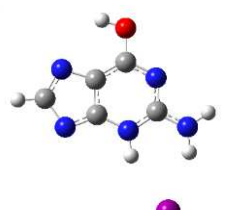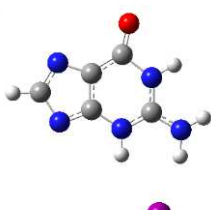
S2 Collision Induced Dissociation
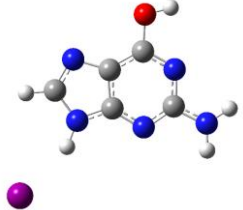
S1 Lowest Energy I⁻·G clusters

The structures of I⁻·G clusters were studied via DFT, at the B3LYP/6-311++G(2d,2p) level of theory on C, N, O, and H, and 6-311G(d,p) on I with the iodine core electrons being described using the Stuttgart/Dresden (SDD) electron core pseudopotential. 3H, 7H and 9H guanine isomers (with H on G3, G7 or G9) were investigated in their keto and enol tautomeric forms. The enolic forms were studied in their cis and trans isomeric forms (with respect to the -NH_2 group), as described in ref. S1. For each of these structures, different iodine positions near the nucleobase were calculated, and the lowest energy ones are shown in Table S1.

Table S1   Calculated structures of the I⁻·G cluster. Calculations were performed were optimised at the B3LYP/6-311++G(2d,2p) level of theory on C, N, O, and H, and 6-311G(d,p)/SDD on I.

Structure	Relative Energy[a] (kJ/mol)	Structure	Relative Energy[a] (kJ/mol)	Structure	Relative Energy[a] (kJ/mol)

I⁻·G7	0	I⁻·G9_E_trans	25.0	I⁻·G7_E_cis	33.0
I⁻·G9	2.43	I⁻·G9_E_cis	28.7	I⁻·G3_E_cis	38.0
I⁻·G7_E_trans	3.45	I⁻·G3_E_trans	31.7	I⁻·G3	40.7

aRelative energies are zero point corrected energies.

26

S2 Collision Induced Dissociation

The fragments associated with ground-state thermal fragmentation were identified *via* collision-induced dissociation (CID) in the ion trap of the amaZon SL (Bruker, Daltoniks) [S2]. Here, selected molecular ions are trapped and accelerate to cause collisions with helium buffer gas and thus fragmentation. The acceleration is obtained by applying a voltage to the end-cap electrode, varying its amplitude between 0 and 10% (2.5 V being the maximum).

CID was performed on the isolated I^-·G cluster and the fragment production curves are shown in Figure S1.

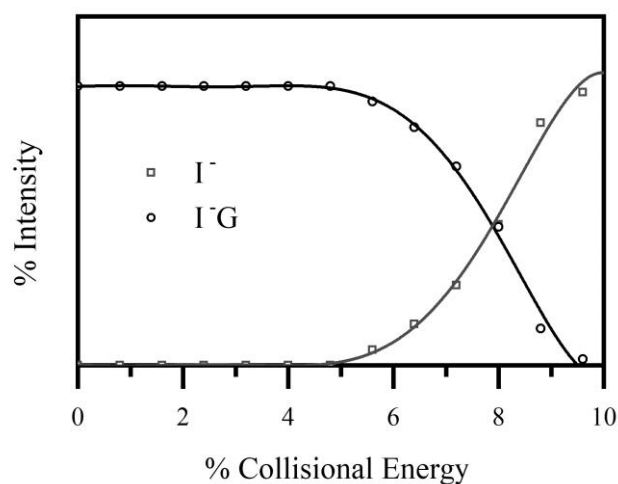Figure S1. Fragment production curves for I^-·G upon CID between 0 and 10 % energy.

References

[S1] G. Chunga, H. Oh and D. Lee, J. Mol. Struct. THEOCHEM **730**, 241 (2005).

[S2] J.N. Louris, R.G. Cooks, J.E.P. Syka, P.E. Kelley, G.C. Stafford Jr. and J.F.J. Todd, Anal. Chem. **59**, 1677 (1987).